Perovskite photovoltachromic cells for building integration

Perovskite photovoltachromic cells for building integration

Alessandro Cannavale,‡[a] Giles E. Eperon,‡[b] Pierluigi Cossari,[a] Antonio Abate,*[b] Henry J. Snaith*[b] and Giuseppe Gigli*[ac]

Photovoltachromic devices combine photovoltaic and electrochromic behaviours to enable adjustable transparency glazing, where the photovoltaic component supplies the power to drive the coloration. Such stand-alone, self-powered devices are of commercial interest for integration into windows and surfaces of buildings and vehicles. Here, we report for the first time a perovskite-based photovoltachromicdevice with self-adaptive transparency. This multifunctional device is capable of producing electrical power by solar energy conversion as well as undergoing a chromic transition from neutral-color semi- transparent to dark blue-tinted when irradiated with solar light, without any additional external bias. Thecombination of semi-transparent perovskite photovoltaic and solid-state electrochromic cells enables fully solid-state photovoltachromic devices with 26% (or 16%) average visible transmittance and 3.7% (or 5.5%) maximum light power conversion efficiency. Upon activating the self-tinting, the average visible transmittance drops to 8.4% (or 5.5%). These results represent a significant step towards the commercialization of photovoltachromic building envelopes.

Introduction

In recent years, the energy market registered a growing demand for photovoltaic technologies (PVs) suitable for building integration.[1,2] Conventional building envelopes, such as roofs and façades, could be replaced by PVs to make energy self-sufficient buildings. This challenging perspective is currently catalysing research activities aiming for new, aesthetically more appealing PVs. In particular, semi-transparent PV modules are strongly desired to replace a number of architectural elements commonly made of glass, such as windows and skylights.[3,4] An ideal PV glazing should be neutral colored and with a tunable level of transparency.[5] Actually, a large choice of colors and high transparency can be easily achieved using dye-sensitized and organic solar cells.[6–10] For example, Hinsch and co-workers demonstrated green-absorbing dye-sensitized modules with a transmittance of around 20% and a solar power conversion efficiency (PCE) of over 7%.[11] Furthermore, amorphous silicon modules have already appeared in the market of semi-transparent PVs a few years ago, though the red or brownish coloring has significantly limited their deployment.[5] More recently, perovskite solar cells[12] have been demonstrated as new potential PV materials for building integration.[13–18] Indeed, semi-transparent perovskite PVs have been reported with tunable visible transmittances between 10 and 50% and PCEs spanning from 5 to 12%.[13,16–18] Moreover, they can be prepared neutral colored offering full flexibility to make aesthetically appealing building integrated PVs.

In addition to mere aesthetic requirements, the transparency and the coloring of glazing building envelopes are critical to control the indoor thermal and visual comfort.[19,20] A number of technologies have been proposed to deliver optically and thermally active building envelopes, which can adaptively modulate the solar radiation and thus the heat gain in buildings. For example, electrochromic windows, currently available in the market, can modulate their throughput of light and thereby heat by applying an external voltage bias.[21,22] Bechinger and co-workers proposed self-powered electrochromic windows, namely photoelectrochromic cells (PECs), where the coloration process is self-generated and it adaptively changes with the external light conditions.[23] In their original architecture,[24,25] PECs were prepared by depositingthe photoactive and the chromogenic electrodes on two glasses separated by a liquid electrolyte. The photoactive electrode was made of a dye-sensitized titanium dioxide layer and the chromogenic electrode was made of a tungsten oxide (WO_3) layer. To activate the coloration, photoexcited electrons are driven to accumulate into WO_3, which becomes opaque after adsorbing positively charged ions from the electrolyte solution.[23] In 2009, Wu and co-workers further advanced this field by integrating PV and PEC technologies in a single device, which is now termed a photovoltachromic cell (PVCC).[26] They demonstrated a self-adaptive transparency of up to 50% - only in the electrochromic central area - and the maximum PCE below 1%. Although PVCCs are some of the most promising device concepts for building-integrated PVs,[27–29] their current PCE is impractical for generating power on a large scale. Furthermore, they are prepared using liquid or gel electrolytes, which is a significant drawback for the processing and the durability.[30–32] To overcome this problem, several efforts have been devoted to the development of solid-state polymer electrolytes (SPEs) which could guarantee a good adhesion between the glass electrodes, high optical transparency, good mechanical properties, simple processability and, most importantly, no issues of leakage or evaporation over time.[33] Efficient SPEs have been prepared using complexes of lithium salts (LiX) and high molecular weight polyethylene oxide (PEO).[34,35] PEO–LiX SPEs showed good ionic conductivity at room temperature, which makes them ideal candidates for application in solid-state PVCCs.

Here, we report a full solid-state perovskite PVCC with self-adaptive transparency and a maximum PCE of over 5%. The device is realized by depositing the photovoltaic (PV) and electrochromic (EC) layers on two separated glass sheets. In Fig. 1a we report a scheme of this new device architecture. The top glass has both sides coated with transparent conductive oxides (TCO), which work as independent electrodes for the PV and EC cells, while the bottom glass has only one side coated with TCO. The PV cell is made of a semi-transparent perovskite deposited on the top TCO glass. The EC layer is made of WO_3 deposited on the bottom TCO glass. A SPE prepared using PEO–LiX and polyethylene glycol (PEG) is used as a glue to laminate the two glasses and complete the EC cell. In Fig. 1, we show pictures of the prototype device with the EC active area completely bleached (b) and colored (c). To activate the coloring, we connected the electrodes as described in Fig. 1a and exposed the device to solar light. Once the coloration has occurred, the PV cell can be used to generate useful power for an external circuit. In a photovoltachromic module, a switch can be used to direct the output of the PV cell as required to either the electrochromic or the external circuit.

Results and discussion

Semi-transparent perovskite was prepared by controlling the film morphology in order to form an ‘island-type’ microstructure as described in our previous work.[13] We encouraged dewetting of the perovskite film from the TCO glass, causing it to form discrete micron-sized islands, indistinguishable to the naked eye. The islands are thick enough to fully absorb the incident light with

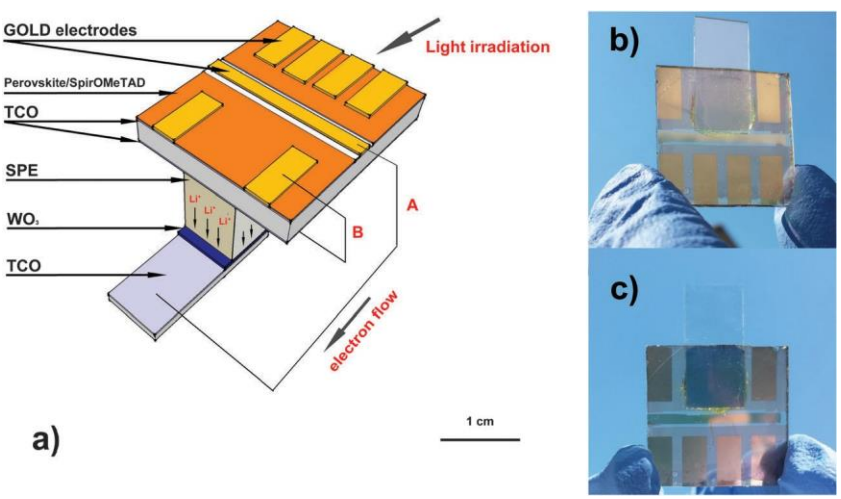

Fig. 1 (a) Axonometric view of the photovoltachromic device. Two external circuits connect the photoanode to the electrochromic electrode (A) and the gold cathode to the secondary electrode of the electrochromic device (B). Pictures of the device under bleached (b) and colored conditions (c) are shown on the right hand side. A schematic describing the coloration mechanism is reported in the ESI.†

an energy above the bandgap of the perovskite semiconductor (B1.57 eV).[12] The combination of fully absorbing islands and fully transparent regions results in an overall homogeneous-looking, semi-transparent and neutral-colored perovskite film (see Fig. 1b and c). We deposited the semi-transparent pero-vskite on TCO glass coated with a compact layer of TiO_2, which acts as an electron collecting layer. Then, chemically doped spiro-OMeTAD (2,2′,7,7′-tetrakis-(*N*,*N*-di-4-methoxyphenylamino)- 9,9′-spirobifluorene)[36,37] was used as a hole collecting layer and gold top electrodes completed the PV cell defining the PV active area (see Fig. 1a).

We fabricated microstructured perovskite films with two different surface coverages, indicating that the ratio of transparent and fully absorbing areas is changed, controlling the overall macroscopic transparency. In Fig. 2, we show the current–voltage characteristics of the PV component of two PVCCs with different transparencies (Samples A and B). The PV performance parameters and the average visible transmittance (AVT) are summarised in Table 1. The AVT is defined as the mean transmittance between 370 nm and 740 nm; in the non- colored state (bleached) it was measured to be 26.1 and 15.9%for the electrochromic areas of Samples A and B, respectively.We note that here light is passing through the solar cell active layer plus the electrochromic cell, but not through the gold electrodes. As already observed in our previous work,[13] the less transparent device (Sample B) displays a significantly higher short-circuit current (J_{sc}) and an overall power conversion effi- ciency (PCE) of 5.5%, compared to a more transmissive devicewith a PCE of 3.7%.

In Fig. 3a we show the bleached/colored transmission spectra of the EC active area for Samples A and B. A maximum bleached/colored modulation of 26 and 12% was observed at 635 nm for Samples A and B, respectively. We also calculated the modulation averaged over the whole visible spectrum (370–740 nm), which was found to be about 18 and 10% for Samples A and B,

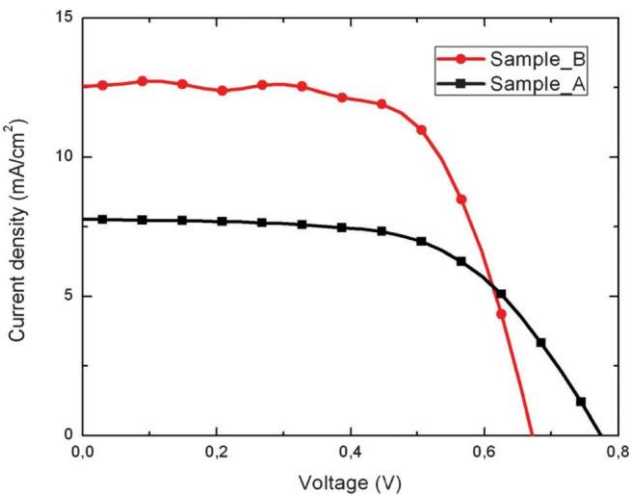

Fig. 2 Current-voltage characteristics for the solar cell layers of the PVCC devices made with two different transparencies. Devices were measured under simulated 100 mW cm^{-2} AM1.5 illumination as detailed in the Experimental section.

Table 1 Photovoltaic performance parameters of PVCCs with two differ- ent transparencies. Open circuit voltage (V_{oc}), short circuit current (J_{sc}) fill factor (FF) power conversion efficiency (PCE) and average visible trans-mittance (AVT)

	V_{oc} (V)	J_{sc} (mA cm^{-2})	FF	PCE (%)	AVT (%)
Sample A	0.77	7.8	0.59	3.7	26.1
Sample B	0.68	12.5	0.63	5.5	15.9

respectively. Though these values are not yet comparable to those reported for electrochromic windows,[22] they are a remark- able result for self-powered devices. We also calculated the AVT after coloration for the electrochromic area of both devices; sample A changes from an AVT of 26.1 (bleached) to 8.4%(colored), and sample B from 15.9 to 5.5%. These are impress-ive changes in the AVT, going from obviously transparent to obviously much more opaque. Clearly sample A, the more trans- parent perovskite sample, will make a more transparent window in the bleached state, but this is at the cost of the photovoltaic performance.

In addition to modular transparency, neutral-coloring is particularly desired in glazing for building integration. To quantify the color of the EC active area and the change it undergoes when transitioning from bleached to colored, we calculated color perception indices according to the CIE 1931 xy color space standard.[36] In Fig. 3b, we plot these color coordinates of the transmission through the whole active region of the devices in both colored and bleached states, compared to the reference daylight illuminant D65 and the AM1.5 spectrum. We observe that the PVCCs in the bleached state have good color-neutrality, lying well within the central region of the chromaticity diagram, close to the AM1.5 spectrum. In the colored state, both devices shift towards the blue side of the color plot. Sample A demonstrates a more extreme change than sample B, as we would expect for a more absorbing sample. Despite shifting towards a bluer color perception, both devices still exhibit color perception close to the centre of the plot, and as such have good color-neutrality, which make them ideal candidates for building integration.

Fig. 4 shows the chronoamperometric measurements of the EC cell in Sample A and Sample B. A voltage of −0.6 V was applied to the electrodes of the EC part of the device. A prompt peak of current (about 2 mA) could be observed in both devices; such a value decreases to roughly 30 mA in about 15–20 s, when the device reaches a stable coloration. Then, the bias was inverted and the bleaching took place with similar kinetics. We reported three complete cycles of coloring/bleaching showing that the coloration process is extremely fast and reproducible in both samples.

We also calculated the electric power absorbed during the coloration process, using the same chronoamperometric curves in Fig. 4. For Sample A, we estimated an initial value of 2.7 mW cm^{-2} (3.8 mW cm^{-2} for Sample B), which decays to zero within 15–20 s, when the coloration is completed. Therefore, the power produced by the PV component (3.7 and 5.5 mW cm^{-2} for Samples A and B, respectively) is thoroughly

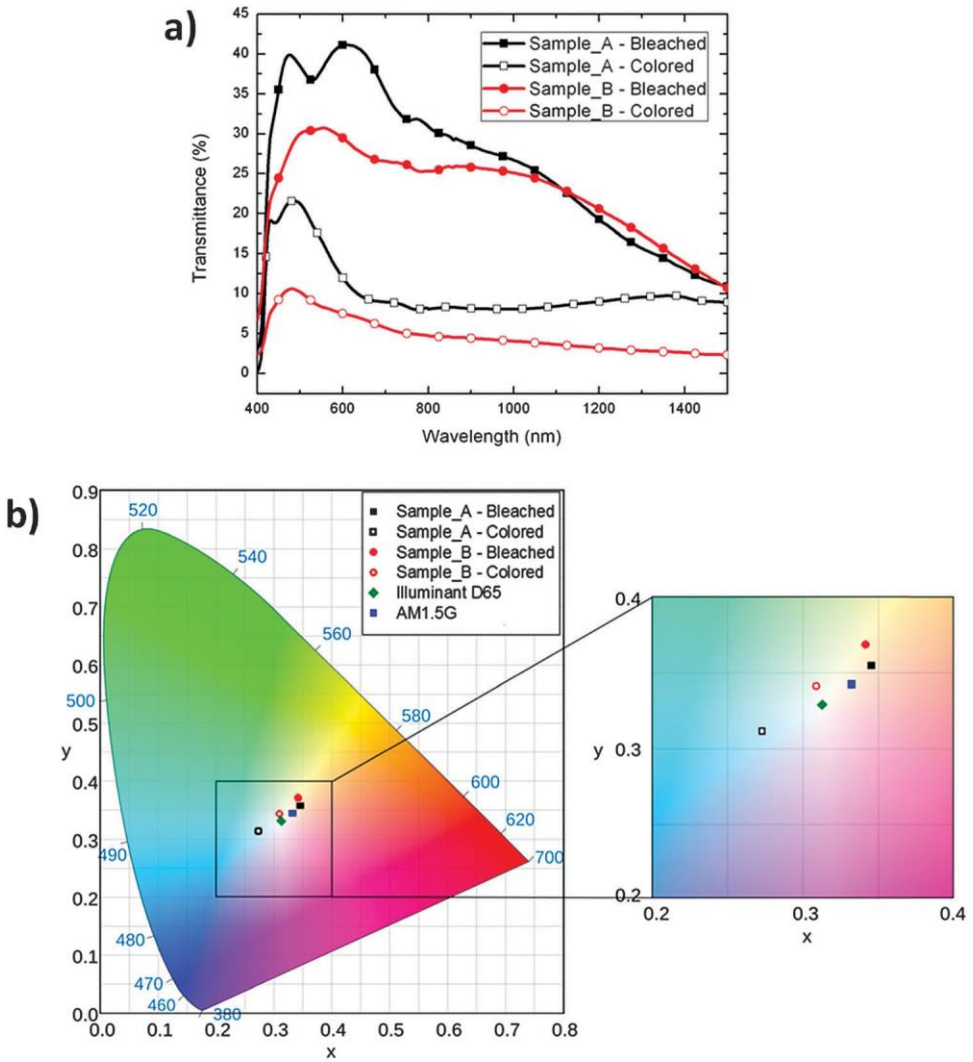

Fig. 3 (a) Transmittance spectra of complete PVCCs (Samples A and Sample B) under bleached and colored conditions in the range of wavelengths between 400 nm and 1500 nm. (b) Color coordinates of the films with transmittance spectra (a) under AM1.5 illumination, plotted on the CIE xy 1931 chromaticity diagram, and the enlarged central region. Color coordinates of the D65 standard daylight illuminant and AM1.5 illumination are also shown.

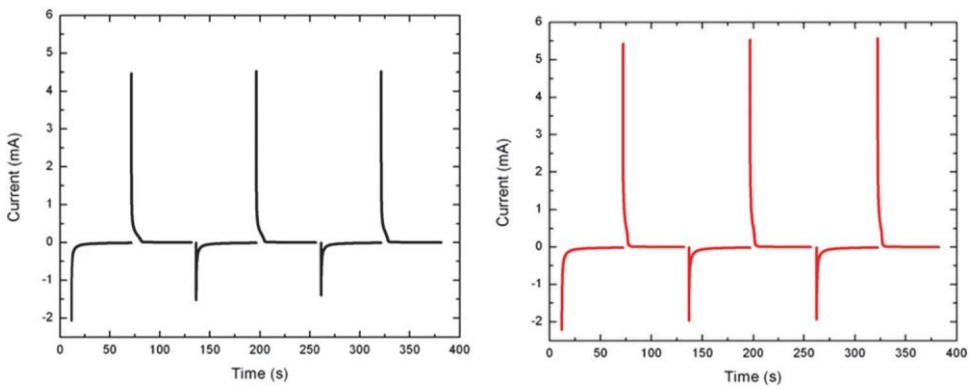

Fig. 4 Chronoamperometric measurements for Sample A (left hand side) and Sample B (right hand side).

sufficient to drive the electrochromic component and it can be used in an external circuit after only 20 s, once the coloration is completed.

To evaluate the quality of our EC cell, we measured the coloration efficiency (CE), which is one of the most commonly used performance parameters.[24] To evaluate CE, we used a well-known

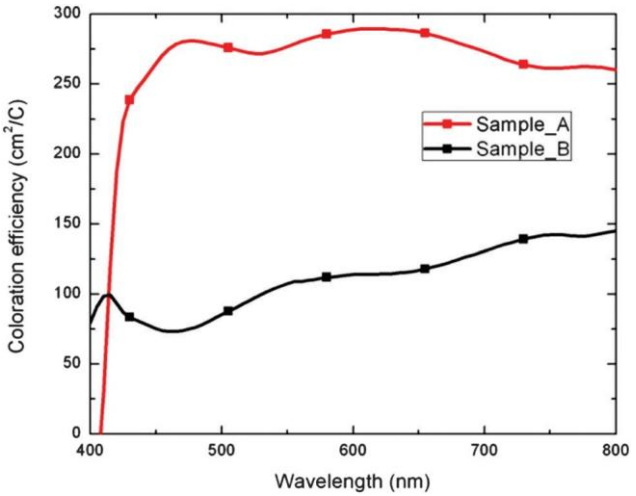

Fig. 5 Coloration efficiency spectra of Sample A and Sample B.

expression relating the efficiency with the optical density, which in turn depends on the transmittances of colored (T_c) and bleached states (T_b), and the insertion charge (Q), as follows:

$$CE = \frac{log\frac{T_b}{T_c}}{Q}$$

The plot for the electrochromic performance is shown in Fig. 5. At a wavelength of 620 nm, the coloration efficiency was determined to be 289 cm^2 C^{-1} for Sample A and 114 cm^2 C^{-1} for Sample B. The higher performance observed for Sample A can be explained taking into account the higher transparency of device A in the bleached state and the lower amount of charge absorbed by Sample A during the coloration (3.3 compared to 4.4 mC for Sample B).

Fig. 6 shows the cyclic voltammogram (CV) of the EC component of the PVCC. The coloring and bleaching associated with WO_3 reduction and oxidation were observed by polarization between −1 and 1 V. A stable current response was achieved after 50 cycles and no significant changes were observed up to

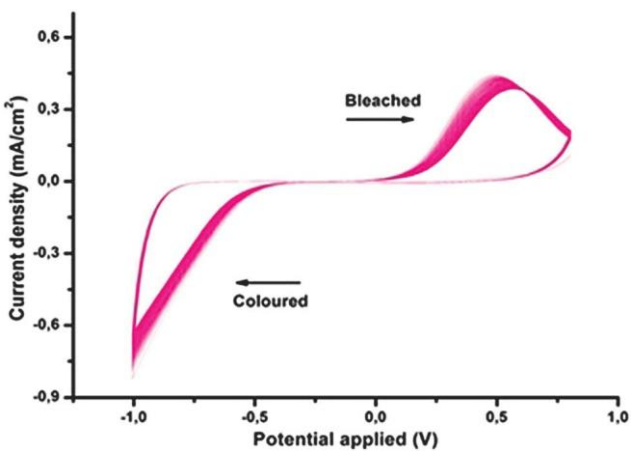

Fig. 6 Cyclic voltammogram of the EC component of the PVCC showing 300 consecutive cycles.

300 cycles, which indicates good electrochemical reversibility and stability within this time window. We highlight that the EC cell was assembled making use of our SPE (see the Experimental section for a detailed formulation) as a glue to laminate the two glass electrodes and no additional sealing was used to protect the device from humid air exposure (see Fig. 1a and b). Further details of the device and the electrolyte stability are given in the ESI.†

Experimental

Electron beam deposition

Tungsten oxide layers (550 nm thick WO_3) were deposited by electron beam deposition on ITO/glass substrates (VisionTech 12 O &$^{-1}$). The vacuum chamber was initially evacuated to 10^{-6} mbar, and then pure dry oxygen was admitted through a needle valve. The pressure was maintained at 10^{-4} mbar throughout the process. The deposition rate was about 1.5 Å s^{-1}. During the deposition process, the chamber reached a temperature of about 215 1C. High vacuum e-beam deposition was also performed to obtain a secondary ITO conductive layer on the FTO glass used for the photovoltaic purposes. In more detail, a 150 nm thick indium tin oxide (Sn:In_2O_3) was used as a conductive layer in order to control the electrochromic functionality of the device. In this case, the vacuum chamber was initially evacuated to 10^{-7} mbar and then a pure dry oxygen flux was admitted througha needle valve. The pressure was maintained at 10^{-4} mbar throughout the deposition. The deposition rate was B0.5 Å s^{-1} and the substrate temperature was maintained at 240 1C during the process. Sheet resistance (20 O &$^{-1}$) was assessed by the four-probe van der Pauw technique.

Photovoltaic cell

Devices were fabricated on the fluorine-doped tin oxide side of the dual TCO coated glass. Initially FTO was removed from regions under the anode contact by etching FTO with 2 M HCl and zinc powder. Substrates were then cleaned sequentially in hellmanex detergent, acetone, propan-2-ol and oxygen plasma. A B50 nm hole-blocking layer of compact TiO_2 was deposited by spin-coating a mildly acidic solution of titanium isopropoxide in ethanol (350 ml in 5 ml ethanol with 0.013 M HCl) at 2000 rpm, and annealed at 500 1C for 30 minutes.

Microstructured perovskite layers were deposited by spin-coating a non-stoichiometric precursor solution of methylammonium iodide and lead chlorine (3 : 1 molar ratio, final concentrations 0.88 M lead chloride, 2.64 M MAI) in anhydrous dimethylsulfoxide (DMSO). To make the more transmissive samples, spin-coating was carried out in ambient air at 2000 rpm for 45 s. These films were then annealed at 130 1C for 20 minutes in ambient air. For the less transmissive samples, spin-coating was carried out in a nitrogen-filled glovebox at 2000 rpm for 45 s. These films were then annealed at 130 1C for 20 minutes in the glovebox.

The hole-transporting layer was then deposited *via* spin-coating a 0.0788 M solution in chlorobenzene of 2,2′,7,7′-tetrakis-(*N*,*N*-di-*p*-methoxyphenylamine)9,9′-spirobifluorene (spiro-OMeTAD),

with additives of 0.0184 lithium bis(trifluoromethanesulfonyl)-imide (added in 0.61 M acetonitrile solution) and 0.0659 M 4-*tert*-butylpyridine. Spin-coating was carried out at 2000 rpmin ambient air.

Gold electrodes were thermally evaporated under vacuum of B10^{-6} Torr, at a rate of B0.1 nm s^{-1} to complete the devices.

Solid polymer electrolyte

Anhydrous lithium iodide (LiI), poly(ethylene oxide) (PEO, M_w = 400 000), poly(ethylene glycol) (PEG, M_w = 400) and acetonitrile (ACN, anhydrous 99.8%) were purchased from Sigma-Aldrich and were used as received. All chemicals were stored in an argon-filled glovebox with o1 ppm H_2O.

The PEO:PEG:LiI electrolyte was prepared with an ether-oxygen to lithium [EO] : [Li^+] molar ratio of 4 : 1, whereas the PEO : PEG weight ratio was fixed as 40 : 60. The homogeneous mixture of PEG and the lithium salt was obtained by stirring the desired concentration of the polymer and the lithium salt for a period of at least 6 hours within a dry argon-filled preparative glovebox. PEO was then dispersed in the PEG–LiI system by adding anhydrous acetonitrile and stirred until it dissolved in the mixture. Finally, the residual solvent was evaporated at room temperature and the polymer electrolyte was dried under vacuum for 72 hours.

Photovoltachromic device fabrication

A small amount of SPE was spread on the WO_3 coated TCO glass and pressed on the second glass to reproduce the architecture reported in Fig. 1a. Mechanical pressure and mild vacuum were applied for 1 hour to laminate the two glass electrodes and remove any residue of air in the electrolyte.

Photovoltaic characterization

The current density–voltage curves were measured (2400 Series SourceMeter, Keithley Instruments) under simulated AM 1.5 sunlight at 100 mW cm^{-2} irradiance generated by an Abet Class AAB sun 2000 simulator, with the intensity calibrated using an NREL calibrated KG5 filtered Si reference cell. The mismatch factor was calculated to be less than 1%. The solar cells were masked with a metal aperture to define the active area of 0.2 cm^2. The current–voltage curves were collected scanning from forward bias to short circuit conditions at 0.38 V s^{-1}. The impact of the hysteresis[37] on the estimated power conversion efficiency has been discussed for similar semi-transparent perovskite devices in our previous publication.[18]

Electro-optical characterization

The optical transmittance spectra of the short-circuited devices were observed using a VARIAN 5000 spectrophotometer in the wavelength range between 400 nm and 1500 nm. Full spectrum measurements were obtained by irradiating the short-circuited devices using an array of seven white Luxeon LEDs (Cool White 6500 K, 7 LED 40 mm–1540 lm at 700 mA), operated by a Keithley source meter. During these measurements, the devices were connected as shown in Fig. 1 using one photovoltaic pixel per time. Chronoamperometry measurements were collected using an Autolab PGSTAT302N (Metrohm AG, the Netherlands) potentiostat.

Electrochemical characterization

Cyclic voltammetry and CA analysis of the EC device were performed using an Autolab PGSTAT 302N in the potential range of 1 V at a scan rate of 1 mV s^{-1}.

Electrochemical impedance spectroscopy (EIS) was carried out using an Autolab PGSTAT302N (Metrohm AG, the Netherlands) combined with a FRA32 frequency generator module by sweeping over 70 points in the frequency range from 10^{-1}–10^6 Hz with a root mean square (RMS) amplitude of 10 mV. The electrolytes with a diameter of 10 mm and a thickness of 50 mm were sandwiched between two stainless steel blocking electrodes separated by a Teflon ring. Impedance spectra were recorded after applying a coloration voltage of 1 V for 10 min in order to reach a steady state. The ionic conductivity (s) was calculated using the relationship $s = l/R_bA$, where l is the thickness of the polymer electrolyte film, A is the contact area between the electrolyte and the electrode, and R_b is bulk resistance obtained from the intercept of the semicircle with the real axis of the Z^0 *versus* Z^{00} Nyquist plot.The calculated ionic conductivity for the PEO–LiX SPE preparedin this work was 1.25 × 10^{-5} S cm^{-1}.

Conclusion

In this work, we report for the first time perovskite PVCCs with self-adaptive transparency. The combination of semi-transparent perovskite photovoltaic and SPE electrochromic cells enables the construction of a full solid-state PVCC with 26% AVT and 3.7% maximum PCE (or 16% AVT and 5.5% maximum PCE), that switches to an AVT of 8.4% (or 5.5%) upon self-activated tinting under illumination. This result represents a significant step towards the commercialization of building-integrated PVCCs, which will allow self-powered tinting windows, with the additional possibility of delivering external power. All of the key components of the system are relatively cheap and the fabrication is compatible with a lamination process, which is well known to the glazing industry. Further advances of our device concept can be achieved by replacing the gold electrodes with semi-transparent top electrodes, which will allow overlap of the photovoltaic and the chromogenic active areas.

Acknowledgements

Dr Vittorianna Tasco and Armando Genco are kindly acknowledged for technical support and beneficial discussions. GE was supported by the EPSRC and Oxford Photovoltaics though a CASE studentship. AA has received funding from the European Union's Seventh Framework Programme for research, technological development and demonstration under grant agreement no. 291771.

References

1 L. El. Chaar and N. El. Zein, *Renewable Sustainable Energy Rev.*, 2011, 15, 2165–2175.
2 P. Heinstein, C. Ballif and L.-E. Perret-Aebi, *Green*, 2013, 3, 125–156.

3 B. P. Jelle, C. Breivik and H. D. Røkenes, *Sol. Energy Mater. Sol. Cells*, 2012, 100, 69–96.
4 C. Peng, Y. Huang and Z. Wu, *Energy Build.*, 2011, 43,3592–3598.
5 P. Boyce, N. Eklund, S. Mangum, C. Saalfield and L. Tang, *Light. Res. Technol.*, 1995, 27, 145–152.
6 B. O'regan and M. Grfitzeli, *Nature*, 1991, 353, 24.
7 C.-C. Chen, L. Dou, R. Zhu, C.-H. Chung, T.-B. Song, Y. B. Zheng, S. Hawks, G. Li, P. S. Weiss and Y. Yang, *ACS Nano*, 2012, 6, 7185–7190.
8 C. C. Chueh, S. C. Chien, H. L. Yip, J. F. Salinas, C. Z. Li, K. S. Chen, F. C. Chen, W. C. Chen and A. K. Y. Jen, *Adv. Energy Mater.*, 2013, 3, 417–423.
9 C. Y. Chang, L. Zuo, H. L. Yip, C. Z. Li, Y. Li, C. S. Hsu, Y. J. Cheng, H. Chen and A. K. Y. Jen, *Adv. Energy Mater.*, 2014, 4.
10 A. Yusoff, R. bin Mohd, S. J. Lee, F. K. Shneider, W. J. da Silva and J. Jang, *Adv. Energy Mater.*, 2014, 4, 1301989.
11 A. Hinsch, W. Veurman, H. Brandt, R. Loayza Aguirre, K. Bialecka and K. Flarup Jensen, *Prog. Photovoltaics*, 2012, 20, 698–710.
12 M. M. Lee, J. Teuscher, T. Miyasaka, T. N. Murakami and H. J. Snaith, *Science*, 2012, 338, 643–647.
13 G. E. Eperon, V. M. Burlakov, A. Goriely and H. J. Snaith, *ACS Nano*, 2013, 8, 591–598.
14 P. Docampo, J. M. Ball, M. Darwich, G. E. Eperon and H. J. Snaith, *Nat. Commun.*, 2013, 4, 2761.
15 J. You, Z. Hong, Y. M. Yang, Q. Chen, M. Cai, T.-B. Song, C.-C. Chen, S. Lu, Y. Liu and H. Zhou, *ACS Nano*, 2014, 8, 1674–1680.
16 C. Roldán-Carmona, O. Malinkiewicz, R. Betancur, G. Longo, C. Momblona, F. Jaramillo, L. Camacho and H. J. Bolink, *Energy Environ. Sci.*, 2014, 7, 2968–2973.
17 L. K. Ono, S. Wang, Y. Kato, S. R. Raga and Y. Qi, *Energy Environ. Sci.*, 2014, 7, 3989–3993.
18 G. E. Eperon, D. Bryant, J. Troughton, S. D. Stranks, M. B. Johnston, T. Watson, D. A. Worsley and H. J. Snaith, *J. Phys. Chem. Lett.*, 2015, 6, 129–138.
19 C. G. Granqvist, A. Azens, P. Heszler, L. Kish and L. Österlund, *Sol. Energy Mater. Sol. Cells*, 2007, 91, 355–365.
20 A. Cannavale, F. Fiorito, D. Resta and G. Gigli, *Energy Build.*, 2013, 65, 137–145.
21 R. D. Rauh, *Electrochim. Acta*, 1999, 44, 3165–3176.
22 R. Baetens, B. P. Jelle and A. Gustavsen, *Sol. Energy Mater. Sol. Cells*, 2010, 94, 87–105.
23 C. Bechinger, S. Ferrere, A. Zaban, J. Sprague and B. A. Gregg, *Nature*, 1996, 383, 608–610.
24 U. O. Krašovec, A. Georg, A. Georg, V. Wittwer, J. Luther and M. Topič, *Sol. Energy Mater. Sol. Cells*, 2004, 84, 369–380.
25 A. Georg and U. O. Krašovec, *Thin Solid Films*, 2006, 502, 246–251.
26 J.-J. Wu, M.-D. Hsieh, W.-P. Liao, W.-T. Wu and J.-S. Chen, *ACS Nano*, 2009, 3, 2297–2303.
27 A. Cannavale, M. Manca, F. Malara, L. De Marco, R. Cingolani and G. Gigli, *Energy Environ. Sci.*, 2011, 4, 2567–2574.
28 A. Cannavale, M. Manca, L. De Marco, R. Grisorio, S. Carallo, G. P. Suranna and G. Gigli, *ACS Appl. Mater. Interfaces*, 2014, 6, 2415–2422.
29 A. L. Dyer, R. H. Bulloch, Y. Zhou, B. Kippelen, J. R. Reynolds and F. Zhang, *Adv. Mater.*, 2014, 26, 4895–4900.
30 A. Abate, A. Petrozza, V. Roiati, S. Guarnera, H. Snaith, F. Matteucci, G. Lanzani, P. Metrangolo and G. Resnati, *Org. Electron.*, 2012, 13, 2474–2478.
31 A. Abate, A. Petrozza, G. Cavallo, G. Lanzani, F. Matteucci, D. W. Bruce, N. Houbenov, P. Metrangolo and G. Resnati, *J. Mater. Chem. A*, 2013, 1, 6572–6578.
32 M.-C. Yang, H.-W. Cho and J.-J. Wu, *Nanoscale*, 2014, 6, 9541–9544.
33 C. G. Granqvist, *Thin Solid Films*, 2014, 564, 1–38.
34 M. J. Reddy, J. S. Kumar, U. S. Rao and P. P. Chu, *Solid State Ionics*, 2006, 177, 253–256.
35 Z. Jia, W. Yuan, H. Zhao, H. Hu and G. L. Baker, *RSC Adv.*, 2014, 4, 41087–41098.
36 R. Hunt and M. Pointer, *Color Res. Appl.*, 1985, 10, 165–179.
37 H. J. Snaith, A. Abate, J. M. Ball, G. E. Eperon, T. Leijtens, N. K. Noel, S. D. Stranks, J. T.-W. Wang, K. Wojciechowski and W. Zhang, *J. Phys. Chem. Lett.*, 2014, 5, 1511–1515.